Geometric dimension assisted absolute phase recovery in 3D shape measurement with digital fringe projection

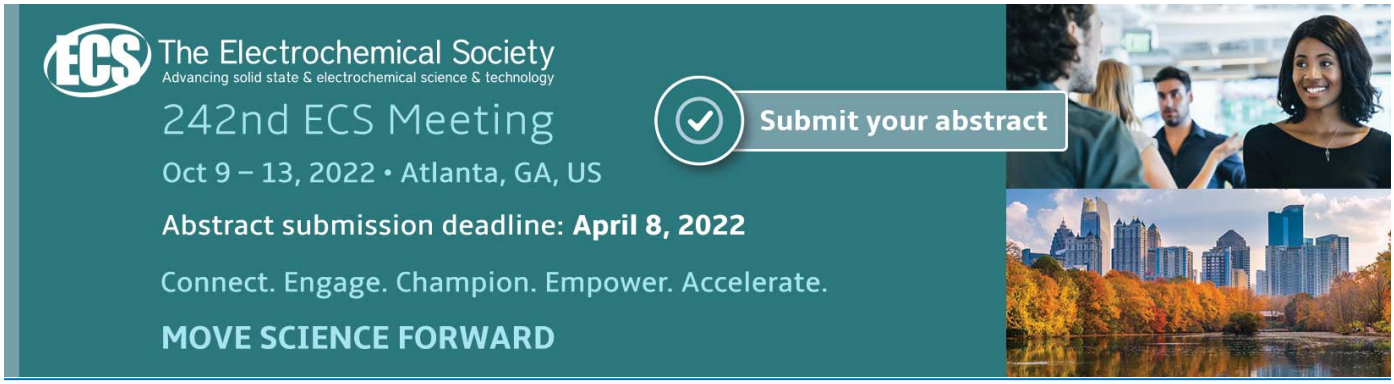

OPEN ACCESS
IOP Publishing
Measurement Science and Technology
Meas. Sci. Technol. **32** (2021) 065001 (9pp)
https://doi.org/10.1088/1361-6501/abd64f

Geometric dimension assisted absolute phase recovery in 3D shape measurement with digital fringe projection

Shenzhen Lv[1,2], Yuyuan Zhang[3], Lei Jing[4], Jian Wang[1], Ying Liu[1] and Qiang Sun[1]

[1] R&D Center of Precision Instruments and Equipment, Changchun Institute of Optics, Fine Mechanics and Physics, Chinese Academy of Sciences, No. 3888, Dongnanhu Road, Changchun, Jilin, People's Republic of China
[2] University of Chinese Academy of Sciences, Beijing 100049, People's Republic of China
[3] College of Science, Jilin Institute of Chemical Technology, Jilin 132022, People's Republic of China
[4] Tianjin University of Technology, No. 391, Tianjin 300384, People's Republic of China

E-mail: sunq@ciomp.ac.cn

Received 27 August 2020, revised 24 November 2020
Accepted for publication 23 December 2020
Published 29 March 2021

Abstract

A novel method of geometric dimension assisted absolute phase recovery in 3D shape measurement is presented. This method mainly includes two steps: (a) using the window Fourier filter-quality guided phase unwrapping algorithm to obtain the relative phase distribution of the tested object; (b) using the geometric dimension of the object as a clue to convert the relative phase distribution to the absolute phase distribution. This method is convenient, and only three fringe image acquisitions are needed to recover the absolute phase. In addition, there is no limit to the depth range of the tested object. The correctness of this method is verified by several experiments.

Keywords: surface measurement, fringe projection, optical metrology, phase unwrapping

(Some figures may appear in color only in the online journal)

1. Introduction

Three-dimensional (3D) shape measurement based on digital fringe projection, which has the merits of fast speed, high accuracy and non-contact measurement, has numerous applications, including industrial online detection, biomedical engineering, computer science, machine vision and reverse engineering [1–4]. In this technique, the fringe patterns are projected to the tested surface for retrieval of the phase distribution containing the 3D shape information of the object. Many phase retrieval methods have been proposed, such as phase-shifting, Fourier transform [5–7], wavelet transform [8], windowed Fourier transform [9, 10] and deep learning [11, 12]. The retrieved phase by the above fringe analysis methods is wrapped within a range from $-\pi$ to π. The wrapped phase needs to be unwrapped to construct a continuous phase distribution. Conventional phase unwrapping methods can be classified into two categories: the spatial phase unwrapping (SPU) and temporal phase unwrapping (TPU).

In SPU, a point in the wrapped phase is selected as the starting point, and then the neighboring pixel points are sequentially unwrapped to achieve a relative phase map. Su and Chen [13] reviewed some quality-guided phase unwrapping algorithms (QGPUs). Compared with other SPU methods

[14], QGPU possesses the advantages of high efficiency, strong robustness and automaticity, and has become the main popular method. Its basic idea is to use a quality map, which reflects the quality of the phase, to guide the phase unwrapping path, so that higher quality phase points are unwrapped before lower quality phase points. Currently, there are many types of quality maps. Zhao *et al* [15] compared the effect of different quality maps in detail, and pointed out that QGPU based on window Fourier transform filtering (WFF) [16] was superior to other kinds of quality maps when dealing with noisy and discontinuous wrapped phases. Although SPU has the advantages of simplicity and convenience, it only provides a relative phase map. As a result, absolute 3D geometry information of a tested object cannot be acquired and multiple separated objects cannot be simultaneously measured.

In TPU, in contrast, the wrapped phase is unwrapped by capturing additional images, and the retrieval of the absolute phase is achieved. Zhang [17] and Zuo *et al* [18] reviewed a variety of TPU methods. Although the absolute 3D geometry information of objects can be acquired by TPU, it is difficult to measure high-speed moving objects due to additional image acquisitions. In addition, for the projection of the fringe patterns with different periods, the corresponding exposure time should be set separately to reduce the impact of noise [19].

Recently, to solve the aforementioned problems, An *et al* [20] proposed an absolute phase unwrapping method based on geometric constraints of the structured light system. In this method, an artificial absolute phase map at a virtual plane with either closest or farthest distance is firstly generated to assist the absolute phase unwrapping [21]. Since no additional image acquisition is required, the measurement speed and quality can be effectively improved. The geometric constraint method has also been applied to other phase recovery fields [22–24]. However, as pointed out in [20], this method has difficulty in measuring objects of greater depth.

In this paper a novel method of geometric dimension assisted absolute phase recovery is presented. Firstly, the WFF-QGPU method [16] is used to obtain the relative phase distribution from three fringe patterns. Then, by running a computer program related to the object dimension (for example, the size along the x or y direction), the relative phase is converted to the absolute phase. Compared with TPU only three fringe image acquisitions are required to recover the absolute phase, which improves the speed of the 3D measurement greatly. Compared with the geometric constraint method, there is no limit to the depth range of the tested object in this method. The effectiveness of the proposed method is demonstrated by several experiments.

The rest of the paper is organized as follows. The principle of the proposed method is introduced in section 2. Section 3 presents several experimental results to validate the method. Section 4 discusses the merits and limitations of the proposed method. Section 5 gives the summary of this paper.

2. Principles

2.1. Three-step phase-shifting algorithm

Among all phase-shifting algorithms, the three-step phase-shifting algorithm requires the minimum number of patterns for the retrieving phase. The fringe patterns can be mathematically written as

$$I_1(x,y) = I'(x,y) + I''(x,y)\cos\left(\Phi(x,y) - \frac{2\pi}{3}\right), \quad (1)$$

$$I_2(x,y) = I'(x,y) + I''(x,y)\cos(\Phi(x,y)), \quad (2)$$

$$I_3(x,y) = I'(x,y) + I''(x,y)\cos\left(\Phi(x,y) + \frac{2\pi}{3}\right), \quad (3)$$

where $I'(x,y)$ is the average intensity, $I''(x,y)$ is the intensity modulation and $\Phi(x,y)$ is the phase to be solved. Solving equations (1)–(3) leads to

$$\phi_{\mathrm{w}}(x,y) = \tan^{-1}\left[\frac{\sqrt{3}(I_1 - I_3)}{2I_2 - I_1 - I_3}\right], \quad (4)$$

$$I_{\mathrm{t}}(x,y) = \frac{I_1 + I_2 + I_3}{3} + \frac{\sqrt{3(I_1 - I_3)^2 + (2I_2 - I_1 - I_3)^2}}{3}, \quad (5)$$

where $\phi_{\mathrm{w}}(x,y)$ is the wrapped phase ranging from $-\pi$ to π, and $I_{\mathrm{t}}(x,y)$ is the texture information which can be used for acquiring the number of pixels of N_y in equation (19) to compute the object geometric dimension of L_{y0} and for image segmentation of multiple objects later.

2.2. Calibration of the system

In this paper, we adopt Zhang and Huang's method [25] for system calibration, in which the projector is regarded as an inverse camera. This method has the advantages of simplicity, simultaneity and high accuracy, and has become a popular calibration method [26]. In this calibration method, a linear pinhole model is used to describe the imaging process of the camera in which the relation between a point of $(x^{\mathrm{w}}, y^{\mathrm{w}}, z^{\mathrm{w}})$ on the object and its projection of $(u^{\mathrm{c}}, v^{\mathrm{c}})$ on the image sensor can be written as

$$s^{\mathrm{c}}[u^{\mathrm{c}}, v^{\mathrm{c}}, 1]^{\mathrm{T}} = P^{\mathrm{c}}[x^{\mathrm{w}}, y^{\mathrm{w}}, z^{\mathrm{w}}, 1]^{\mathrm{T}}, \quad (6)$$

$$P^{\mathrm{c}} = A^{\mathrm{c}}[R^{\mathrm{c}}, t^{\mathrm{c}}], \quad (7)$$

where s^{c} is a scale factor, the superscript c denotes the camera, the superscript w denotes the world coordinates, A^{c} is the intrinsic matrix of the camera, and R^{c} and t^{c} are the camera's extrinsic matrices. Similarly, the pinhole model of the projector is as follows:

$$s^{\mathrm{p}}[u^{\mathrm{p}}, v^{\mathrm{p}}, 1]^{\mathrm{T}} = P^{\mathrm{p}}[x^{\mathrm{w}}, y^{\mathrm{w}}, z^{\mathrm{w}}, 1]^{\mathrm{T}}, \quad (8)$$

$$P^{\mathrm{p}} = A^{\mathrm{p}}[R^{\mathrm{p}}, t^{\mathrm{p}}], \tag{9}$$

where the superscript p denotes the parameters of the projector. In this study, the camera's coordinate system is selected as the world coordinate system, and so the projection matrices of the camera and projector can be respectively expressed as,

$$P^{\mathrm{c}} = \begin{bmatrix} f_u^{\mathrm{c}} & 0 & u_0^{\mathrm{c}} & 0 \\ 0 & f_v^{\mathrm{c}} & v_0^{\mathrm{c}} & 0 \\ 0 & 0 & 1 & 0 \end{bmatrix} \text{ and}$$
$$P^{\mathrm{p}} = \begin{bmatrix} f_u^{\mathrm{p}} & 0 & u_0^{\mathrm{p}} \\ 0 & f_v^{\mathrm{p}} & v_0^{\mathrm{p}} \\ 0 & 0 & 1 \end{bmatrix} \begin{bmatrix} r_{11} & r_{12} & r_{13} & t_1 \\ r_{21} & r_{22} & r_{23} & t_2 \\ r_{31} & r_{32} & r_{33} & t_3 \end{bmatrix}, \tag{10}$$

where f_u^{c} and f_v^{c} are the focal lengths of the camera lens along the u and v directions, respectively, and $(u_0^{\mathrm{c}}, v_0^{\mathrm{c}})$ is the camera's principle point coordinate. Here, f_u^{p} and f_v^{p} are the focal lengths of the projector lens along the u and v directions, respectively, and $(u_0^{\mathrm{p}}, v_0^{\mathrm{p}})$ is the principle point coordinate of the projector. Here, r_{ij} and t_i are the elements of the rotation and translation matrices, respectively.

There are seven unknown parameters of $(u^{\mathrm{p}}, v^{\mathrm{p}}, x^{\mathrm{w}}, y^{\mathrm{w}}, z^{\mathrm{w}}, s^{\mathrm{c}}, s^{\mathrm{p}})$ in equations (6) and (8) which provide only six equations. Generally, to acquire the 3D shape information of an object, another equation is provided by the recovery of the absolute phase from the captured fringe patterns. The projector pixel coordinates of u^p and v^p can be determined by the following equations,

$$u^{\mathrm{p}} = \frac{\Phi^{\mathrm{V}}(u^{\mathrm{c}}, v^{\mathrm{c}})}{2\pi} T, \tag{11}$$

$$v^{\mathrm{p}} = \frac{\Phi^{\mathrm{H}}(u^{\mathrm{c}}, v^{\mathrm{c}})}{2\pi} T, \tag{12}$$

where Φ^{V} and Φ^{H} are the absolute phase maps along the vertical and horizontal directions, respectively, and T is the fringe period. Without losing generality, we take the vertical fringe patterns for analysis. Solving equations (6)–(10) simultaneously leads to

$$z^{\mathrm{w}} = \frac{f_u^{\mathrm{c}}[(u^{\mathrm{p}} - u_0^{\mathrm{p}})t_3 - f_u^{\mathrm{p}} t_1]}{f_u^{\mathrm{c}}[f_u^{\mathrm{p}} r_{13} - (u^{\mathrm{p}} - u_0^{\mathrm{p}})r_{33}] + (u^{\mathrm{c}} - u_0^{\mathrm{c}})[f_u^{\mathrm{p}} r_{11} - (u^{\mathrm{p}} - u_0^{\mathrm{p}})r_{31}] + (v^{\mathrm{c}} - v_0^{\mathrm{c}})[f_u^{\mathrm{p}} r_{12} - (u^{\mathrm{p}} - u_0^{\mathrm{p}})r_{32}]}, \tag{13}$$

$$x^{\mathrm{w}} = \frac{u^{\mathrm{c}} - u_0^{\mathrm{c}}}{f_u^{\mathrm{c}}} z^{\mathrm{w}}, \tag{14}$$

$$y^{\mathrm{w}} = \frac{v^{\mathrm{c}} - v_0^{\mathrm{c}}}{f_v^{\mathrm{c}}} z^{\mathrm{w}}. \tag{15}$$

2.3. Geometric dimension assisted absolute phase recovery

We know that there is a relationship between the relative unwrapped phase and the absolute unwrapped phase, which can be expressed as

$$\Phi_{\mathrm{abs}} = \Phi_{\mathrm{rel}} + 2\pi n, n \in z, \tag{16}$$

where Φ_{abs} denotes the absolute phase, Φ_{rel} represents the relative phase and Z denotes an integer. In this paper, the relative phase is obtained by WFF-QGPU, where the detailed process can be found in [16]. Therefore, if we can determine the value of n, then we can convert the relative phase to the absolute phase. The process of the determination of the n value is as follows.

Firstly, we analyze the range of the value of n. According to equation (11), the range of the absolute phase distribution of the generated fringe pattern is from 0 to $\frac{2\pi}{T} u^{\mathrm{p}}_{\mathrm{max}}$, with $u^{\mathrm{p}}_{\mathrm{max}}$ being the number of pixels of the projector in the u^{p} direction. In general, negative values in the relative phase obtained by the WFF-QGPU method exist, and the true absolute phase distribution is always greater than 0. So the lower limit of n is:

$$n_1 = \left[-\frac{\min(\Phi_{\mathrm{rel}})}{2\pi} \right], \tag{17}$$

where [] means the integer function and min() denotes the function of taking the minimum value. Similarly, the upper limit of n must make the maximum value of equation (16) less than $\frac{2\pi}{T} u^{\mathrm{p}}_{\mathrm{max}}$. Therefore, the upper limit of n is:

$$n_2 = \left[\frac{u_{\mathrm{max}^{\mathrm{p}}}}{T} \right] - \left[\frac{\max(\Phi_{\mathrm{rel}})}{2\pi} \right], \tag{18}$$

where max() represents the function of taking the maximum value.

Secondly, we calculate $L_x(n)$ and $L_y(n)$, the object dimensions in the x and y directions corresponding to different n values. It can be seen from equation (13) that the depth coordinate of z^{w} of the object is a function of the projector pixel coordinate of u^{p}, and u^{p} is determined by the absolute phase distribution of the object given in equation (11). Therefore, as the value of n varies in the defined range, the calculated depth distribution of z^{w} varies correspondingly. On the other hand, the x^{w} and y^{w} coordinates of the object are directly related to the z^{w} coordinates, and so the calculated object dimensions of $L_x(n)$ and $L_y(n)$ vary with respect to n values. Therefore, the information of the size of the object along the x or y direction can be used as a new clue to determine the correct n value. Although we adopt the size of the object along the y direction in this paper, it is also feasible to adopt it along the x direction.

Thirdly, we calculate $DL_y(n)$, the difference between $L_y(n)$ and L_{y0} for different values of n, where L_{y0} is the previously acquired object dimension in the y direction. According to the imaging relationship in geometric optics, L_{y0} can be calculated by the following equation,

$$L_{y0} = N_y \delta \frac{s}{f'}, \tag{19}$$

where N_y denotes the number of pixels on the camera sensor corresponding to the object in the y direction given by the texture information of $I_t(x,y)$ in equation (5), δ is the camera sensor unit size, s represents the object distance from the object to the camera lens and f' denotes the focal lengths of the camera lens. In the experiments in this paper, according to the calibrated object space ranging from 627 mm to 700 mm in the depth direction, we always place the tested object close to the plane of 627 mm in the depth direction, and so we set the object distance of s to be 630 mm.

Fourthly, we seek out the correct value of n giving a minimized value of $DL_y(n)$ from the constructed data set.

The specific process is as shown in the code below, where abs () represents the function of taking the absolute value, and find () represents the function of finding the position of a specific element from a known data set

for n from n_1 to n_2

$$\Phi(n) = \Phi_{\text{rel}} + 2\pi n,\ u^{\text{p}} = \frac{\Phi(n)}{2\pi} T$$

$$z(n) = \frac{f_u^{\text{c}}[(u^{\text{p}} - u_0^{\text{p}})t_3 - f_u^{\text{p}} t_1}{f_u^{\text{c}}[f_u^{\text{p}} r_{13} - (u^{\text{p}} - u_0^{\text{p}})r_{33}] + (u^{\text{c}} - u_0^{\text{c}})[f_u^{\text{p}} r_{11} - (u^{\text{p}} - u_0^{\text{p}})r_{31}] + (v^{\text{c}} - v_0^{\text{c}})[f_u^{\text{p}} r_{12} - (u^{\text{p}} - u_0^{\text{p}})r_{32}]}$$

$$y(n) = \frac{v^{\text{c}} - v_0^{\text{c}}}{f_v^{\text{c}}} z(n)$$

$$L_y(n) = \max(y(n)) - \min(y(n))$$

$$DL_y(n) = \text{abs}(L_y(n) - L_{y0})$$

end

$$n = \text{find}(DL_y(n)) = \min(DL_y(n))$$

Finally, the absolute phase map is recovered by substituting the determined n into equation (16). Figure 1 shows the entire procedure.

3. Experiments

We build a hardware system to verify the performance of the proposed method. This system includes a camera (DAHENG MER-131-210U3M-L) that is attached with a 12.5 mm lens and a projector (DLP6500). The projector's resolution is 1080 × 1920 pixels, and the camera's resolution is 1024 × 1280 pixels with the size of the sensor unit being 4.8 μm × 4.8 μm.

We firstly validate the proposed method by measuring a single star object shown in figure 2(a). The number of pixels of the star in the y direction of N_y is 892, which is acquired with the texture information of $I_t(x,y)$ in equation (5). Figure 2(b) is one of the three-step phase-shifting fringe patterns acquired by the camera, where the fringe period of T is 40 pixels. The wrapped phase of the object is calculated by equation (4), and then an exponential fringe pattern is generated. The WFF method is used to process the generated exponential fringe pattern, as described in [16]. The filtered phase and amplitude are shown in figures 2(c) and (d), respectively. The filtered phase is unwrapped by the WFF-QGPU method. Figure 2(e) is the unwrapping path, and figure 2(f) is the unwrapped phase. The unwrapping process is from light yellow pixels to dark red pixels in figure 2(e) successively.

Then, we apply the proposed method in section 2.3 to convert the relative phase to the absolute phase. Firstly, the limits of n are calculated using equations (17) and (18). The acquired lower limit of n_1 is 15 and the upper limit of n_2 is 36. Substituting the value of N_y into equation (19), we get the star object dimension of L_{y0}, which is 216 mm. Then, by running the program described in figure 1, the dimension of $L_y(n)$ and the difference of $DL_y(n)$ are obtained as different values of n being taken during the process. The distribution of $DL_y(n)$ with respect to n values is shown in figure 3(a). It can be seen that $DL_y(n)$ takes the minimum value when n is equal to 22. Substituting the determined value of n into equation (16), the absolute phase distribution is obtained, which is shown in figure 3(b). We then investigate the error tolerance of the object distance of s in yielding the correct value of n. It is found by simulations that the allowable range of s is from 621 mm to 648 mm, indicating the effectiveness of the setting of s in this research.

Figure 4(a) is the 3D shape measurement result obtained by the proposed method. To verify whether the above result is correct, we also perform the 3D shape measurement of the same star using the TPU method, the enhanced two-frequency phase-shifting method (ETM) [22]. The adopted fringe periods

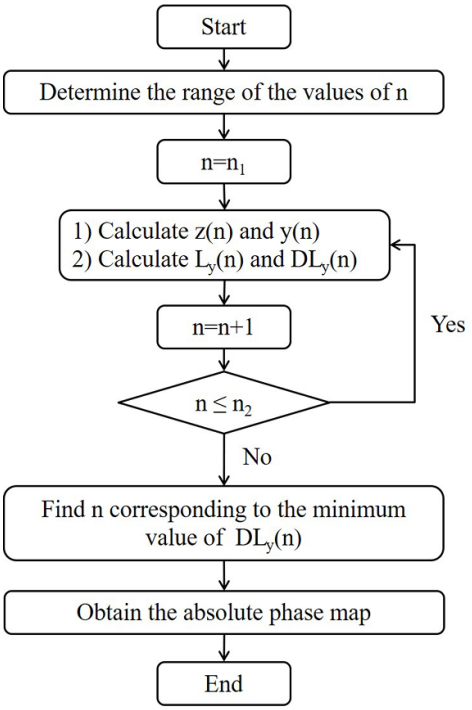

Figure 1. A flowchart of the whole geometric dimension assisted absolute phase recovery.

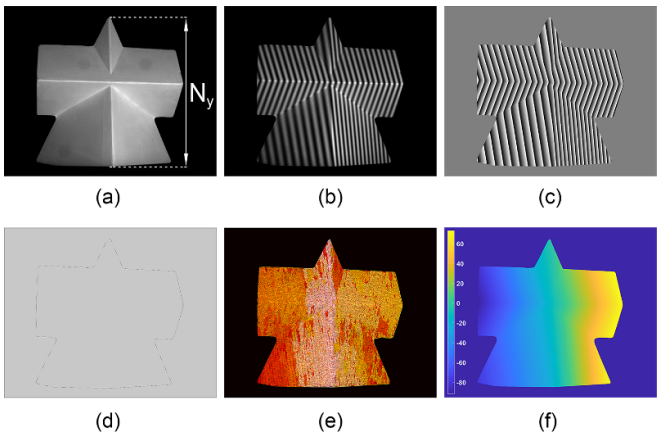

Figure 2. Phase unwrapping of the star using WFF-QGPU. (a) A single star object (N_y = 892); (b) one of the three-step phase-shifting fringe patterns (T = 40 pixels); (c) the filtered phase map using WFF; (d) the filtered amplitude map using WFF; (e) the unwrapping path map; (f) the relative phase map of the star object.

are 40 and 270 pixels, and the phase-shifting consists of three steps. The 3D shape measurement result obtained by ETM is shown in figure 4(b). Then, we calculate the difference between figures 4(a) and (b) point by point, and the depth difference map is shown in figure 4(c) which has RMS values of 0.08 mm, proving the correctness of the proposed method in achieving absolute phase recovery.

To further evaluate the performance of the proposed method, a more complex object shown in figure 5(a) is used as the tested object in the experiment. The fringe period of

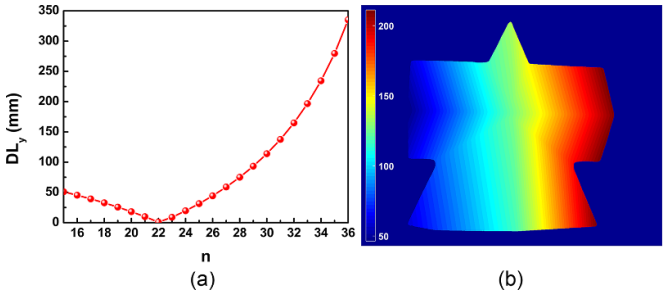

Figure 3. Convert the relative phase to absolute phase using the proposed method. (a) Distribution of the difference of $DL_y(n)$ during the process; (b) the absolute phase map acquired by the proposed method.

the three-step phase-shifting patterns is 80 pixels on the image sensor. The number of pixels of the complex object in the y direction of N_y is 611, and so the dimension of L_{y0} is 148 mm. Figure 5(b) is the relative phase distribution obtained by the WFF-QPGU method. Similarly, the limits of n are calculated, and the acquired lower limit of n_1 and the upper limit of n_2 are 3 and 20, respectively. By running the program, $L_y(n)$ and $DL_y(n)$ are obtained as different values of n being taken during the process. Figure 5(c) shows the distribution of $DL_y(n)$ with respect to n values. It can be seen that $DL_y(n)$ takes the minimum value when n is equal to 12. Figure 5(d) shows the obtained absolute phase distribution by substituting an n value of 12 into equation (16). It is found that the allowable variation range of s in this case is from 601 mm to 653 mm. It can be seen, in a comparison with the last experiment, that the larger the fringe period, the greater the error tolerance of the object distance setting is.

We further compare the performance of the ETM and the proposed method on the complex object. Figure 6(a) is the 3D shape measurement result obtained by the proposed method and figure 6(b) is that obtained by the ETM, where the adopted two fringe periods are 80 and 270 pixels with the phase-shifting of three steps. We calculate the difference between figures 6(a) and (b) point by point, and the depth difference map is shown in figure 6(c). The depth difference distribution has an RMS value of 0.151 mm, which is quite small, indicating that the depth image acquired by the proposed method is of absolute phase distribution.

Finally, the experiment of 3D shape measurement of two separated objects shown in figure 7(a) is carried out using the proposed method, and the process is as follows. Firstly, the texture information given by equation (5) is used to create two masks for segmenting each individual object. The masks are shown in figures 7(b) and (c). Secondly, the relative phase for each individual object is obtained using the WFF-QGPU method, and the acquired relative phase distributions are shown in figures 7(d) and (e). Thirdly, the method described in section 2.3 is used to convert the relative phase into the absolute phase for each object, and the acquired absolute phase distributions are shown in figures 7(f) and (g). Finally, the absolute phase distribution of the separated

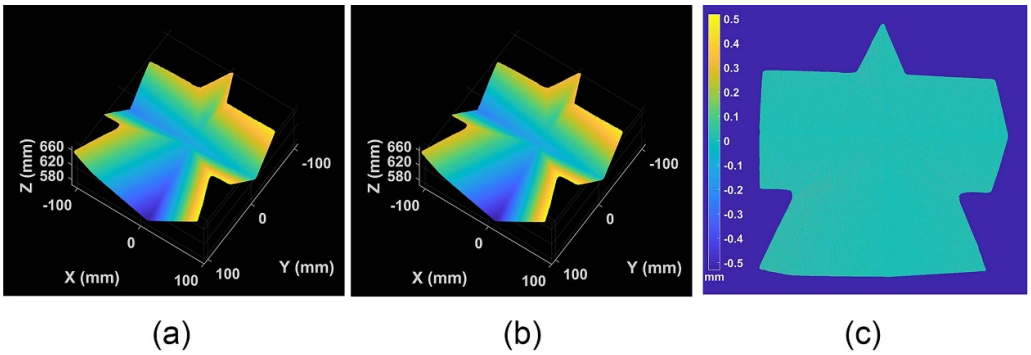

Figure 4. Experimental results of the star object. (a) The 3D shape measurement result acquired by the proposed method; (b) the 3D shape measurement result acquired by ETM; (c) the map of the depth difference between figures (a) and (b) (RMS = 0.08 mm).

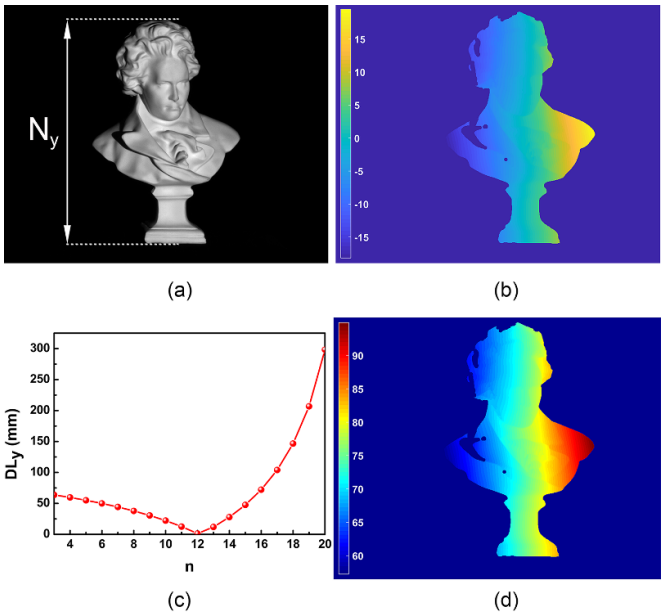

Figure 5. The 3D shape measurement of a complex object. (a) The tested complex object image ($N_y = 611$); (b) the relative phase map of the complex object acquired by WFF-QGPU ($T = 80$ pixels); (c) the distribution of the difference of $DL_y(n)$ during the process; (d) the absolute phase map of the complex object acquired by the proposed method.

objects is acquired by integrating the absolute phase distributions in figures 7(f) and (g) together, which is shown in figure 7(h).

The parameters converting the relative phase into the absolute phase for each of the objects are as follows. For the first object, the dimension of $L1_{y0}$ is 148 mm. The calculated lower limit of n_1 is 2 and the upper limit of n_2 is 19. For the second object, the dimension of $L2_{y0}$ is 149 mm. The calculated lower limit of n_1 is 2 and the upper limit of n_2 is 19. Figure 8(a) shows the acquired $DL_y(n)$ with respect to n values during the process for the first object, and figure 8(b) shows this for the second object. It should be pointed out that the abscissa in figure 8(a) does not end from the upper limit of 19, since the last few values of $DL_y(n)$ are very large. We can see that the value of n giving the minimum value of $DL_y(n)$ is 7 for the first object, and it is 15 for the second object. With the acquired n values the absolute phase distributions are obtained.

Again, the 3D shape measurement result of the separated objects obtained by the proposed method is compared with that obtained by ETM. Figure 9(a) is the 3D shape map obtained by the proposed method, and figure 9(b) is that obtained by ETM. We also calculate the difference between figures 9(a) and (b) point by point, and the depth difference map is shown in figure 9(c). Figure 9(c) has an RMS value of 0.156 mm, which is also quite small, indicating that the depth image acquired by the proposed method is of absolute phase distribution.

4. Discussion

The proposed absolute phase recovery method has the following advantages and limitations.

4.1. High-speed 3D shape measurement

Unlike traditional TPU methods, this method only needs three fringe image acquisitions for absolute phase recovery, and thus it is more suitable for high-speed measurement. If the approximate lateral size of the tested object is already known, the estimation of the object's lateral size will no longer be needed with the proposed method. This makes it more convenient in applications such as circuit board inspection and defect detection.

4.2. Robustness to noise

Window Fourier transform is a redundant transform, and its spectrum reflects the local characteristics of a signal. Thereby, the noise in the wrapped phase map can be well suppressed.

4.3. Simple system setup

The method does not require an additional camera for absolute phase unwrapping, and can be directly employed by the single-projector and single-camera structured light system.

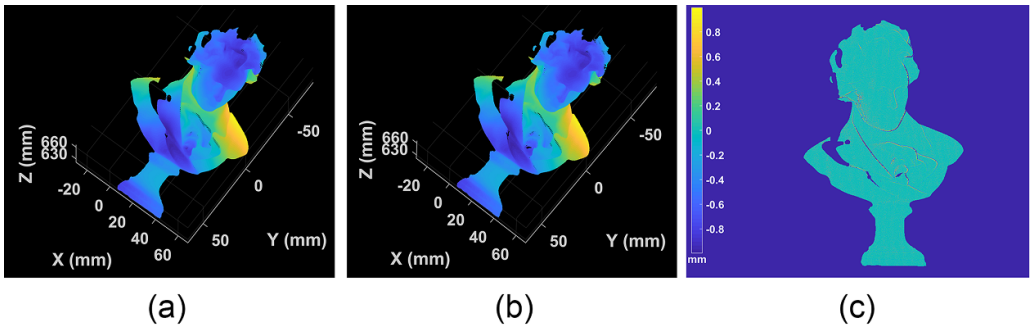

Figure 6. Experimental results of the complex object. (a) The 3D shape measurement result acquired by the proposed method; (b) the 3D shape measurement result acquired by ETM; (c) the map of the depth difference between figures (a) and (b) (RMS = 0.151 mm).

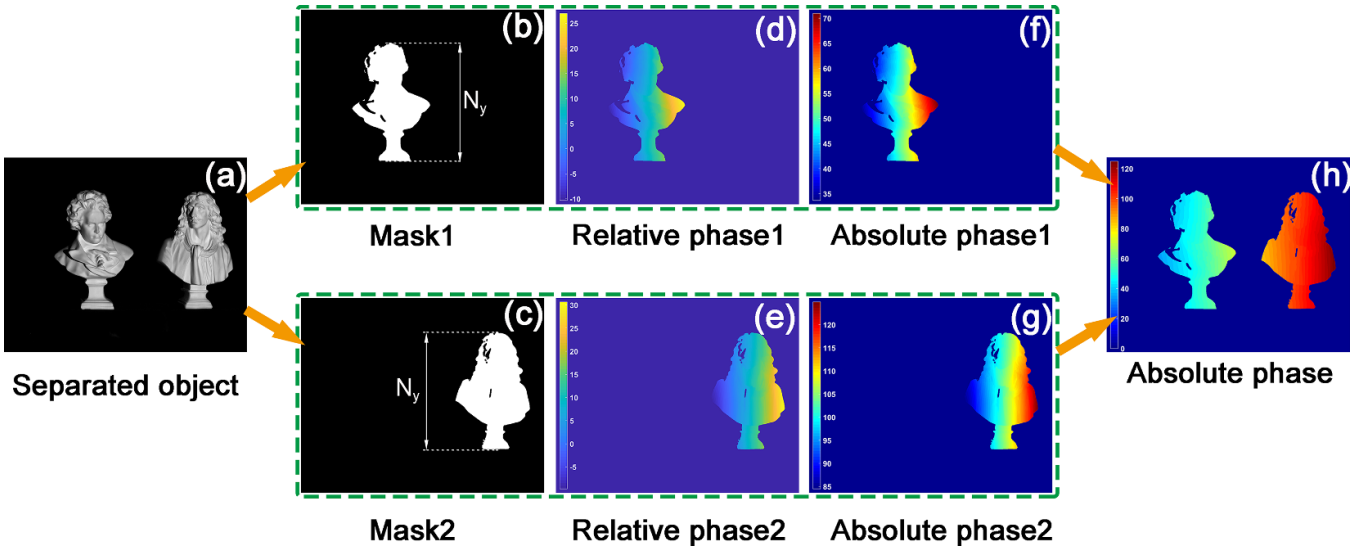

Figure 7. A flow process diagram of the absolute phase retrieval for two separated objects. (a) The image of two separated objects; (b) the mask of the first object ($N_y = 611$); (c) the mask of the second object ($N_y = 614$); (d) the relative phase map of the first object acquired by WFF-QGPU ($T = 80$ pixels); (e) the relative phase map of the second object acquired by WFF-QGPU ($T = 80$ pixels); (f) the absolute phase of the first object acquired by the proposed method; (g) the absolute phase of the second object acquired by the proposed method; (h) the absolute phase distribution of the tested objects acquired by integrating the phase distributions in (f) and (g) together.

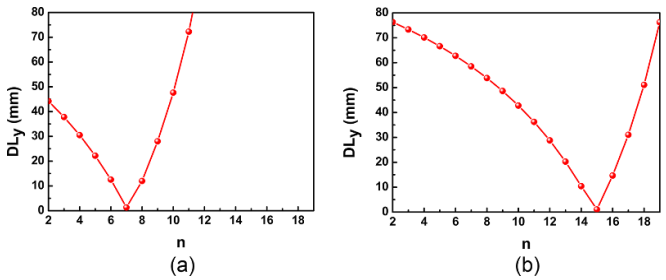

Figure 8. The distributions of $DL_y(n)$ in the process for the two separated objects; (a) the distribution of $DL_y(n)$ for the first object; (b) the distribution of $DL_y(n)$ for the second object.

4.4. No confined measurement depth range

In the depth-constrained method, the virtual absolute phase distribution at the selected virtual plane is calculated first and then the virtual absolute phase distribution is used as a reference in the phase unwrapping to construct a continuous absolute phase distribution of the object. With this method, however, the difference between the virtual phase distribution and the continuous phase distribution of the object should be less than 2π in principle, leading to the depth limitations of the tested object [20]. With the proposed method, the lateral size of the object is only used as a constraint condition to convert the relative phase to the absolute phase distribution of the object, and therefore there is no limitation to the measurement depth range.

4.5. Limitations and solutions

WFF-QGPU adopted in this paper is a type of SPU method and thus limitations exist in the measurement of objects with abrupt geometric discontinuities. The object's surface geometry, at least one unwrapping path, should not introduce more than π phase changes between two successive points. However, we found in our actual experiments that the limitation could be alleviated by changing the angle of the

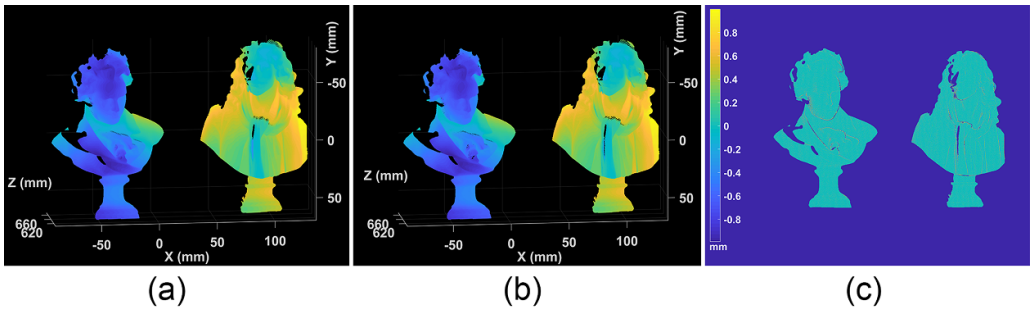

Figure 9. The 3D measurement results of two separated objects. (a) The 3D shape measurement result acquired by the proposed method; (b) the 3D shape measurement result acquired by ETM; (c) the map of the depth difference between figures (a) and (b) (RMS = 0.156 mm).

fringe pattern (i.e. from the vertical to horizontal orientation), or by increasing the period of the fringe pattern appropriately.

5. Conclusions

A novel method of geometric dimension assisted absolute phase recovery in a structured light system is presented in this paper. Compared with TPU only three fringe image acquisitions are required to recover the absolute phase, which is beneficial to the speed and accuracy of 3D shape measurement. Compared with the geometric constraint method, there is no limit to the depth range of the tested object. The limitations to the tested objects of geometric discontinuities with this method is discussed and the solutions are given. The correctness and effectiveness of this method are verified by several experiments.

Acknowledgments

The authors would like to acknowledge the support of the National Key Research and Development Project (2018YFC0308100 and 2018YFC0307900), and the Projects of Science Technology Development Plan of Jilin Province under Grant (20190302102GX).

ORCID iD

Shenzhen Lv https://orcid.org/0000-0003-4112-5208

References

[1] Gorthi S S and Rastogi P 2010 Fringe projection techniques: whither we are? *Opt. Lasers Eng.* **48** 133–40
[2] Marrugo A G, Gao F and Zhang S 2020 State-of-the-art active optical techniques for three-dimensional surface metrology: a review [Invited] *J. Opt. Soc. Am.* A **37** 60–77
[3] Zhong M, Cui J, Hyun J-S, Pan L, Duan P and Zhang S 2020 Uniaxial three-dimensional phase-shifting profilometry using a dual-telecentric structured light system in micro-scale devices *Meas. Sci. Technol.* **31** 085003
[4] Heist S, Dietrich P, Landmann M, Kuhmstedt P, Notni G and Tunnermann A 2018 GOBO projection for 3D measurements at highest frame rates: a performance analysis *Light Sci. Appl.* **7** 71
[5] Takeda M and Mutoh K 1983 Fourier transform profilometry for the automatic measurement of 3D object shapes *Appl. Opt.* **22** 3977–82
[6] Su X and Chen W 2001 Fourier transform profilometry *Opt. Lasers Eng.* **35** 263–84
[7] Liu Y, Zhang Q, Zhang H, Wu Z and Chen W 2020 Improve temporal Fourier transform profilometry for complex dynamic three-dimensional shape measurement *Sensors* **20** 1808
[8] Zhong J and Weng J 2005 Phase retrieval of optical fringe patterns from the ridge of a wavelet transform *Opt. Lett.* **30** 2560–2
[9] Qian K 2007 Two-dimensional windowed Fourier transform for fringe pattern analysis: principles, applications and implementations *Opt. Lasers Eng.* **45** 304–17
[10] Qian K 2004 Windowed Fourier transform for fringe pattern analysis *Appl. Opt.* **43** 2695–702
[11] Rivenson Y, Zhang Y, Gunaydin H, Teng D and Ozcan A 2018 Phase recovery and holographic image reconstruction using deep learning in neural networks *Light Sci. Appl.* **7** 17141
[12] Feng S, Chen Q, Gu G, Tao T, Zhang L, Hu Y, Yin W and Zuo C 2019 Fringe pattern analysis using deep learning *Adv. Photonics* **1** 025001
[13] Su X and Chen W 2004 Reliability-guided phase unwrapping algorithm: a review *Opt. Lasers Eng.* **42** 245–61
[14] Ghiglia D and Pritt M 1998 *Two-Dimensional Phase Unwrapping: Theory, Algorithms, and Software* (New York: Wiley)
[15] Zhao M, Huang L, Zhang Q, Su X, Asundi A and Qian K 2011 Quality-guided phase unwrapping technique: comparison of quality maps and guiding strategies *Appl. Opt.* **50** 6214–24
[16] Qian K, Gao W and Wang H 2008 Windowed Fourier-filtered and quality-guided phase-unwrapping algorithm *Appl. Opt.* **47** 5420–8
[17] Zhang S 2018 Absolute phase retrieval methods for digital fringe projection profilometry: a review *Opt. Lasers Eng.* **107** 28–37
[18] Zuo C, Huang L, Zhang M, Chen Q and Asundi A 2016 Temporal phase unwrapping algorithms for fringe projection profilometry: a comparative review *Opt. Lasers Eng.* **85** 84–103
[19] Zhang S 2020 Rapid and automatic optimal exposure control for digital fringe projection technique *Opt. Lasers Eng.* **128** 106029
[20] An Y, Hyun J S and Zhang S 2016 Pixel-wise absolute phase unwrapping using geometric constraints of structured light system *Opt. Express* **24** 18445–59
[21] Lv S, Sun Q, Zhang Y, Wang J and Jiang Y 2020 Monotonicity analysis of absolute phase unwrapping by geometric constraint in a structured light system *Opt. Express* **28** 9885–98
[22] Hyun J S and Zhang S 2016 Enhanced two-frequency phase-shifting method *Appl. Opt.* **55** 4395–401

[23] Li B, An Y and Zhang S 2016 Single-shot absolute 3D shape measurement with Fourier transform profilometry *Appl. Opt.* **55** 5219–25
[24] Hyun J-S and Zhang S 2020 High-speed three-dimensional absolute shape measurement with three projected binary patterns *Opt. Eng.* **59** 0241041–8
[25] Zhang S and Huang P S 2006 Novel method for structured light system calibration *Opt. Eng.* **45** 083601–8
[26] Lv S, Sun Q, Zhang Y, Jiang Y, Yang J, Liu J and Wang J 2019 Projector distortion correction in 3D shape measurement using a structured-light system by deep neural networks *Opt. Lett.* **45** 204–7